



Hydrologic regimes drive nutrient export behavior in human impacted watersheds

Galen Gorski¹, Margaret A. Zimmer¹

¹Department of Earth and Planetary Sciences, University of California Santa Cruz, Santa Cruz, CA, 95064, United States

Correspondence to: Galen Gorski (ggorski@ucsc.edu)

Abstract. Agricultural watersheds are significant contributors to downstream nutrient excess issues. The timing and magnitude of nutrient mobilization in these watersheds are driven by a combination of anthropogenic, hydrologic, and biogeochemical factors that operate across a range of spatial and temporal scales. However, how, when, and where these complex factors drive nutrient mobilization has previously been difficult to capture with low-frequency or spatially limited datasets. To address this knowledge gap, we analyzed daily nitrate concentration (c) and discharge (Q) data for a four-year period (2016-2019) from five nested, agricultural watersheds in the midwestern United States that contribute nutrient loads to the Gulf of Mexico. The watersheds span two distinct landforms shaped by differences in glacial history resulting in natural soil properties that necessitated different drainage infrastructure across the study area. To investigate nutrient export patterns under different hydrologic conditions, we partitioned the hydrograph into stormflow and baseflow periods and examined those periods separately through the analysis of their concentration-discharge (c - Q) relationships on annual, seasonal, and event time scales. Stormflow showed consistent chemostatic patterns across all seasons, while baseflow showed seasonally dynamic c - Q patterns. Baseflow exhibited chemodynamic conditions in the summer and fall and more chemostatic conditions in the winter and spring, suggesting that water source contributions during baseflow were nonstationary. Baseflow chemodynamic behavior was driven by low-flow, low- NO_3^- conditions during which in-stream and near-stream biological processing likely moderated in-stream NO_3^- concentrations. Additionally, inputs from deeper groundwater with longer residence times and lower NO_3^- concentration likely contributed to low- NO_3^- conditions in-stream, particularly in the larger watersheds. Stormflow c - Q behavior was consistent across watersheds, but baseflow c - Q behavior was linked to intensity of agriculture and density of built drainage infrastructure, with more drainage infrastructure associated with higher loads and more chemostatic export patterns across the watersheds. This suggests that how humans ‘replumb’ the subsurface in response to geologic conditions has implications for hydrologic connectivity, homogenization of source areas, and subsequently nutrient export during both baseflow and stormflow. Our analysis also showed that anomalous flow periods greatly influenced overall c - Q patterns, suggesting that the analysis of high-resolution records at multiple scales is critical when interpreting seasonal or annual patterns.

1 Introduction

Excess nutrient export to streams can have detrimental effects on human health and ecosystem function, by contaminating drinking water (Weyer et al., 2001) and contributing to harmful algal blooms (Howarth, 2008), hypoxia



(Jenny et al., 2016) and loss of species diversity in receiving water bodies (Diaz & Rosenberg, 2008). Globally, the
35 number of hypoxic dead zones that have been identified in the scientific literature has roughly doubled each decade,
now reaching well over 500 (Conley et al., 2011). The spatial extent and severity of dead zones are often correlated
to temporal patterns in upstream nitrogen loading from contributing catchments (Rabalais et al., 2009; Turner et al.,
2012).

One of the largest dead zones in the world is in the northern Gulf of Mexico, which experiences expansive
40 eutrophication each spring and summer due to nutrient export from largely agricultural watersheds within the Upper
Mississippi River Basin (Rabalais et al., 2002). In response, many US states have invested considerable resources in
developing nutrient reduction strategies with the goal of mitigating nutrient mobilization and downstream effects. For
example, the Iowa Nutrient Reduction Strategy has a goal of reducing nitrogen loads in Iowa streams by 45%,
committing \$560 million to meet that goal in 2019 alone (*Iowa Nutrient Reduction Strategy: 2018-19 Annual Progress*
45 *Report*, 2020).

Despite the considerable investments in developing solutions, downstream water bodies still receive
substantial nitrogen loading from their upstream watersheds (Bouraoui & Grizzetti, 2011; Sprague et al., 2011). One
reason for this persistence is the buildup of applied nitrogen that can remain in the subsurface for decades and
contribute to in-stream nitrate (NO_3^-) loads long after application practices have changed, or mitigations strategies
50 have been implemented (Fovet et al., 2015; Sebiló et al., 2013). These, and other NO_3^- sources create a heterogeneous
patchwork of source areas throughout the landscape that can become “activated” or “deactivated” in response to
changing hydrologic conditions (Abbott et al., 2018; Dupas et al., 2019). A better understanding of what factors
contribute to source area activation, and the timing of their activation is critical to predicting in-stream NO_3^-
concentrations and loads and ultimately developing operational nutrient management strategies.

An effective method for investigating contributing source zones within a watershed is the examination of the
55 relationship between solute concentration and stream discharge (c-Q relationships) (e.g. Godsey, 2009; Thompson et
al., 2011). When viewed in log-log space, solute concentration and discharge often vary linearly according to a slope,
which can be used to describe the relative tendency of a watershed to transport or retain the solute under various
hydrologic conditions (Basu et al., 2010; A. Musolff et al., 2017). Slopes near zero ($|\text{c-Q slope}| \leq 0.2$) indicate
60 chemostatic behavior in which solute concentration varies little in response to changes in discharge. Chemostatic
conditions can arise when contributing areas have uniform solute concentrations, as is often seen with NO_3^- in areas
with intensive agriculture (Bieroza et al., 2018; Thompson et al., 2011). In contrast, chemodynamic behavior is
characterized by slopes different from zero in which the solute concentration is sensitive to changes in discharge.
Chemodynamic conditions can arise from source areas with more heterogeneous solute concentrations which may
65 become activated under different hydrologic conditions (Dupas et al., 2019). The c-Q relationship can be characterized
as an enrichment pattern if the slope is positive (c-Q slope > 0.2) or a dilution pattern if the slope is negative (c-Q
slope < -0.2).

Recent studies have recognized that c-Q relationships vary as a function of flow percentile, suggesting that
the structure of hydrologic connectivity is driven by flow conditions (Diamond & Cohen, 2018; Jones et al., 2017;
70 Zimmer et al., 2019). Recently, the accessibility of data from high-frequency sensor networks has allowed the



exploration of these relationships at a time scale previously difficult to observe. For example, high-frequency datasets have been used to investigate c-Q behavior at the event scale, revealing dynamic changes in NO_3^- sourcing and processing at short timescales (Blaen et al., 2017; Bowes et al., 2015; Carey et al., 2014). However, much previous work has focused on a single catchment, and/or data collected over a relatively short period of time. This makes it difficult to determine how the connections between the hydrologic, biogeochemical, and anthropogenic factors, which operate over a range of temporal and spatial scales, influence in-stream NO_3^- concentrations. For example, antecedent moisture conditions, and precipitation timing and intensity reflect changes that occur over hours or days (Rozemeijer et al., 2010), while vegetation dynamics, and on-farm practices such as crop planting and fertilization reflect seasonal changes (Minaudo et al., 2019; Royer et al., 2006). Additionally, the influence of these factors are impacted by differences in watershed-specific characteristics, such as topography, soil type, land use practices, and geologic history (Marinos et al., 2020; Moatar et al., 2017). Understanding how these processes and watershed characteristics interact across the relevant spatial and temporal scales in heavily managed watersheds is a crucial step in developing strategies to mitigate downstream impact (Hansen et al., 2018).

Only recently have high-resolution records become sufficiently long and instrumentation sufficiently widespread to examine c-Q relationships under different hydrologic conditions in multiple locations. With this, we are now able to identify how streamflow and NO_3^- concentration relationships vary annually and seasonally across key spatial gradients. Here, we analyze four years of publicly available daily measurements of discharge and NO_3^- concentration from five nested agricultural watersheds in the midwestern United States. Using a semi-autonomous event picking algorithm, we partition the hydrograph into stormflow and baseflow periods to address the following research questions:

- 1) How do c-Q relationships during stormflow and baseflow periods vary by season, and what can that tell us about changes in hydrologic connectivity and nitrogen sources throughout the year?
- 2) What relationship do NO_3^- concentration, load measurements, and c-Q relationships have to underlying and human-impacted watershed properties?
- 3) How can high-frequency records be used to identify distinct export regimes and characterize anomalous events that might play a disproportionate role in watershed c-Q behavior?

2 Methods

2.1 Site description

The Raccoon River watershed drains 8,870 km² of low-relief, heavily agricultural area in central Iowa, USA, which drains into the Gulf of Mexico (Figure 1). It is made up of the North Raccoon River watershed (USGS HUC: 07100007) and the South Raccoon River watershed (USGS HUC: 07100006).

For this study we subdivided the Raccoon River watershed into a series of five nested watersheds shown in Figure 1; the Upstream Sac City (*USC*) and the Middle Redfield (*MRF*) on the North Raccoon River, the Upstream Panora (*UPN*) on the Middle Raccoon River, the Middle Jefferson (*MJF*) on the South Raccoon River, and the



Downstream Van Meter (*DVM*), which is below the confluence of the three major tributaries draining the area. The *MJF* is inclusive of *USC*; *MRF* is inclusive of *UPN*, and *DVM* is inclusive of the entire Raccoon River watershed. Typical of this area, agricultural productivity is the dominant land use in all five watersheds ranging from 85-92% of
110 land use (Table S2), the vast majority of which is corn (*Zea mays L.*) and soybeans (*Glycine max L.*).

The Raccoon River watershed is marked by a stark divide in landforms driven by recent glaciations, with the majority of the area underlain by glacial sediments deposited by the Des Moines Lobe during the last glaciation of the region approximately 12,000 years ago (Prior, 1991). These areas are characterized by poorly developed surface drainage networks and ephemeral surface water bodies. As a result, extensive tile drainages, ditches, and canals have
115 been installed and constructed in the latter half of the 20th century to drain excess water from the subsurface (Figure 1). The southwestern portion of the Raccoon River watershed lies within the Southern Iowa Drift Plain, an area that was shaped by 500,000-year-old glacial advances that extended south into present day Missouri (Prior, 1991). This portion of the watershed is characterized by steeper topography and more naturally well-developed drainage networks, which require less drainage infrastructure such as tile drains, ditches, and canals. *UPN*, *MRF*, and *DVM* drain areas
120 that overlay both the Des Moines Lobe and the Southern Iowa Drift Plain.

The Raccoon River watershed is characterized by cold dry winters and warm wet summers, with an average annual precipitation of 850 mm (1981-2010; PRISM), the majority of which falls as rain between April and October, aligning with the growing season.

2.2 Datasets

We analyzed in situ mean daily NO_3^- concentration (c) and discharge (Q) data from the outlet of each watershed at gaging stations maintained by the U.S. Geologic Survey for *USC* (05482300), *MRF* (05483600), *MJF* (05482500), and *DVM* (05484500), and from the Iowa Institute of Hydraulic Research (IIHR) for *UPN* (WQS0032). To retrieve data, we used the dataRetrieval package in R (v 3.6.0) through the National Water Information System (De Cicco et al., 2018). Data for *UPN* was obtained directly from the IIHR. We analyzed daily discharge and NO_3^-
130 concentration data from January 2016 to December 2019, during which discharge records were complete for all sites and NO_3^- records had > 88% coverage for all sites except *UPN*, which had 72% coverage (Table S1). At each gaging station, NO_3^- concentrations were measured at 15-minute resolution (5-min for *UPN*) using Hach Nitratax plus sc probes (Hach, Loveland, CO) and aggregated to daily average NO_3^- concentration for this study.

To analyze land use characteristics for each watershed, we downloaded land use data from the National
135 Landcover Database 2016 at a 30 m x 30 m resolution (Dewitz, 2019). Land use data were binned into four categories; water/wetlands, developed, forested/barren/shrubs, and crops (including pasture). Data for landforms, drainage infrastructure, and stream network were downloaded from the Iowa Department of Natural Resources. We downloaded daily precipitation data for the four-year period of analysis (2016-2019) for two sites (*USC00137312* and *USC00136566*) within the Raccoon River watershed from the NOAA National Centers for Environmental
140 Information.



2.3 Event identification

We separated the discharge time series into baseflow and stormflow periods through semi-automating storm event identification using the following criteria: 1) $dQ/dt \geq 1e-4$ cfs/second for the rising limb of the event, 2) $\max(Q_{\text{event}}) \geq 0.01 * \max(Q_{\text{record}})$, and 3) the event duration ≥ 3 days. The end of each event was determined when either the event falling limb $dQ/dt \geq 0$ or discharge returned to pre-event levels. For some, such as events that showed up as shoulder peaks on larger events, or those with indistinct peaks, visual inspection and subjective decisions were required (Figure S1). The criteria were derived from similar studies (Dupas et al., 2016; Knapp et al., 2020; Rozemeijer et al., 2010), and exact thresholds for the criteria were tuned and adapted for the structure and dynamics of the watersheds' hydrographs to ensure the selection of peaks. Time periods identified as storm events were classified as stormflow, and all other times were classified as baseflow (Figure 2).

We note that this classification scheme differs from traditional baseflow separation techniques that use graphical, geochemical or isotopic approaches to identify and separate the proportion of the hydrograph that is comprised by baseflow and stormflow (Hooper & Shoemaker, 1986; Klaus & McDonnell, 2013). Baseflow separation techniques have shown that a large fraction of event water is derived from baseflow (e.g. Schilling & Zhang, 2004). Our goal is not to contradict or supplant this finding, but rather to illustrate how a simple partitioning of the hydrograph based on peaks in discharge allows us to isolate nutrient export dynamics in specific hydrologic regimes.

2.4 Characterizing export regimes

Export patterns (chemostatic, dilution, or enrichment) were calculated for stormflow, baseflow, and the full record (herein referred to as stormflow+baseflow) for the full period of analysis and on a seasonal basis. Concentration-discharge relationships for baseflow and stormflow+baseflow periods were calculated by aggregating data for the time period of interest. Stormflow c-Q relationships were calculated in two ways; first by aggregating data from all stormflow events over the time period of interest, and second, by calculating c-Q relationships for each individual storm event and averaging those values over all events (Figure S4). The former is referred to as bulk stormflow c-Q relationships, and the later as event-averaged c-Q relationships.

Seasonal and annual calculations were made based on the water year which begins on October 1st, and the year was divided seasonally into fall (October, November, December), winter (January, February, March), spring (April, May, June), and summer (July, August, September).

2.5 Load estimations

Cumulative NO_3^- load estimates were calculated for each hydrologic regime (stormflow, baseflow, stormflow+baseflow) on an annual and seasonal basis as:

$$\sum_{i=1}^n c_i Q_i / f \quad (1)$$

where c_i and Q_i are the daily NO_3^- concentration and discharge values, and f is the fraction of data coverage for the period of interest. If data were missing during a period, baseflow and stormflow loads were calculated based on their



fractional contribution during the periods with data. All annual periods had $f > 0.75$, but some seasonal periods had low coverage, for seasonal periods where $f \leq 0.75$ no load estimate was calculated.

180

3 Results and discussion

3.1 Stream flow exhibits strong seasonality

In all five watersheds, 44-52% of the analysis period was classified as stormflow, with an average of 15 unique storm events in each watershed per year (Table 1). While the proportion of stormflow periods was similar between watersheds, the fraction of flow that was partitioned into stormflow and baseflow varied considerably between watersheds. *MJF* and *USC* had the highest proportion of stormflow, with 77.0 and 73.4% of annual flow classified as stormflow, respectively, compared to 62.4 and 63.9% in *UPN* and *MRF*, respectively (Table 1). This observation is consistent with the higher density of drainage infrastructure (e.g. canals, tile drainage) in *MJF* and *USC*, leading to quicker routing of high flows to the stream channel compared to more natural drainage networks in *UPN* and *MRF*.

190

Flow in all watersheds exhibited strong seasonality, with an average of 42.9% of total flow delivered in the spring. Summer months contributed the least to overall discharge with an average of 17.3% across all watersheds. Despite differences in overall flow between the seasons, spring and summer experienced a similar number of stormflow events across all watersheds (average of 5.5 in spring and 4.4 in summer; Student's t-test; $p > 0.01$), and similar precipitation totals (average 309 mm in spring and 381 mm in summer; Student's t-test; $p > 0.01$). Increased streamflow in the spring months is likely a result of snow melt, rain on snow events, which can produce excess runoff, and increased crop growth in the summer months leading to more water retention.

195

3.2 NO_3^- concentrations are sensitive to watershed characteristics, season, and hydrologic regime

The outlet of the largest watershed (*DVM*) showed median NO_3^- concentrations of 7.38 ± 3.07 mg/L. The heavily tile-drained *USC* watershed showed the highest median NO_3^- concentration (9.23 ± 3.09 mg/L), while *MRF*, which has the least drainage infrastructure, showed the lowest (6.96 ± 2.51 mg/L; Table S3). This is consistent with observations of increased stream NO_3^- concentrations at the outlets of heavily tile-drained Iowa watersheds compared to those with less built drainage infrastructure (Schilling et al., 2012).

200

NO_3^- concentrations exhibited pronounced seasonality in both stormflow and baseflow, with annual minima during the summer and maxima during the spring (Figure 3). Summer baseflow NO_3^- concentrations correlated well with watershed area as the outlet of the largest watershed experienced the lowest concentration (Figure 3A). Low NO_3^- concentrations in summer are often associated with lower flow periods which may have increased contributions from groundwater flow paths with longer residence times, and more streambed-water interaction, both positively associated with watershed area (Peralta-Tapia et al., 2015). In addition, summer periods have warmer temperatures, which promote biological nitrogen uptake activity (e.g. denitrification and assimilation) that can lower NO_3^- concentrations (Moatar et al., 2017; Rode et al., 2016). Weakened correlations between baseflow NO_3^- concentrations and watershed area during the rest of the year suggest that other processes may be more effective at driving NO_3^- concentrations at other times of the year.

205

210



215 Maximum NO_3^- concentrations were observed in the spring during both baseflow and stormflow periods
(Figure 3). During stormflow periods, NO_3^- concentrations correlated positively with drainage infrastructure density
during all seasons, but the correlation was strongest during the spring months when the NO_3^- concentrations were
highest (Figure 3B). During spring precipitation events, water infiltrates rapidly through relatively bare soils,
encountering accumulated nitrogen stocks in the shallow subsurface from previous years or early season fertilizer
220 application and is routed off the landscape through tile drains (Van Meter et al., 2020; Royer et al., 2006). High flow
periods can also reduce the ability of biological processes to alter NO_3^- concentrations (Rodríguez-Blanco et al., 2015;
Royer et al., 2006). This seasonality of NO_3^- concentration has been previously observed in the Raccoon River
watershed (K. Schilling & Zhang, 2004), as well as other agricultural catchments in the Midwest (Dupas et al., 2017;
Van Meter et al., 2020; Pellerin et al., 2014).

225

3.3 Baseflow c-Q patterns reveal seasonally shifting nitrate processing and sources

Concentration-discharge relationships showed a difference between baseflow and bulk stormflow periods,
with baseflow periods exhibiting generally more chemodynamic c-Q slopes (Figure 4). Enriching chemodynamic
export patterns (c-Q slope > 0.2) were observed during baseflow periods in all watersheds annually, with *UPN* showing
230 the strongest enrichment signal (c-Q slope = 0.79) and *USC* showing the weakest (c-Q slope = 0.21) (Figure 4A).
Baseflow c-Q slopes were seasonally dynamic with the fall and summer experiencing generally higher c-Q slopes
(blue and red triangles, respectively; Figure 4A), and winter and spring c-Q slopes closer to zero (green and yellow
triangles, respectively; Figure 4A). There is a negative correlation between seasonal baseflow c-Q slope and drainage
infrastructure density, which is strongest during the spring months ($R^2 = 0.85$; Table S4). During these months, positive
235 baseflow c-Q slopes are driven by low flow, low NO_3^- concentration periods, which are less prevalent in the
watersheds with a higher density of drainage infrastructure (*USC*, *MJF*, and *DVM*). The lack of low NO_3^-
concentration periods in these watersheds results in chemostatic c-Q slopes as the built drainage infrastructure serves
to homogenize baseflow sources.

These human impacts can be highlighted by comparing the two end member watersheds in our dataset. *MRF*,
240 which has the lowest density of drainage infrastructure (0.37 km/km^2), experienced chemodynamic enriching c-Q
slopes across all seasons during baseflow, ranging from 0.34 in the winter to 0.75 in the summer. This suggests highly
heterogeneous source regions contributed to baseflow throughout the year. In contrast, *USC*, which has the highest
density of drainage infrastructure (1.11 km/km^2) experienced chemodynamic conditions only in the summer (c-Q
slope = 0.29), and chemostatic conditions across the other seasons. This suggests there were consistent, homogeneous
245 sources producing stable NO_3^- concentrations across a range of flow conditions throughout the year.

The strongest chemodynamic enrichment patterns occurred in the summer across all watersheds, while the
most chemostatic season was generally the spring (Figure 4). This pattern is exemplified in *DVM*, which integrates
the signal from the other four upstream watersheds (Figure 2E). The summer baseflow period in *DVM* is strongly
enriching (c-Q slope = 0.75), while in spring, baseflow is chemostatic (c-Q slope = 0.08). This dynamic shift is driven
250 by differences in baseflow NO_3^- concentrations from spring to summer, suggesting differences in the sourcing or
internal processing of baseflow from one season to the next (Richardson et al., 2020).



3.4 Stormflow c-Q patterns show stationarity in seasonal NO₃⁻ sources

Bulk stormflow periods generally exhibited more chemostatic behavior than baseflow periods (Figure 4).
255 The observation that low flow periods were more chemodynamic than high flow periods is consistent with other
studies that have partitioned the hydrograph seasonally (Ehrhardt et al., 2019), by breakpoint analysis (Marinos et al.,
2020), or by median discharge (Moatar et al., 2017), suggesting that this is a general feature of watershed hydrologic
routing. Bulk stormflow c-Q slope exhibited subtle seasonality with a slight dilution trend in winter c-Q slopes in
several watersheds, and a slight enrichment trend in spring and summer (Figure 4B). Fall bulk stormflow c-Q slopes
260 were chemostatic to weakly chemodynamic for all watersheds except *UPN*, which showed a c-Q slope of 0.71. This
higher c-Q slope was driven by two anomalous, low NO₃⁻ concentration events discussed in further detail in Section
3.5.

Although tile drained watersheds show higher stormflow NO₃⁻ concentrations (Figure 3B), there does not
appear to be a systematic effect on stormflow c-Q slopes (Figure 4B). This indicates that the nitrate sources activated
265 during stormflow periods are transport-limited across all watersheds. That is, regardless of season, storms contribute
flow to streams generally through shallow, quick flow paths that intersect high-NO₃⁻ stores in these agriculturally
intensive landscapes (Buda & DeWalle, 2009; Mellander et al., 2012).

Analysis of individual storm events reveals that event-averaged c-Q slopes form a narrow distribution around
zero across all seasons (Figure 5A). Although many individual events could be classified as strongly chemodynamic
270 if considered in isolation, examining the events in aggregate shows that there is a tendency towards chemostatic
behavior across all watersheds (Figure 5B and S4). The comparison of bulk stormflow c-Q slopes (Figure 4B) and
event averaged c-Q slopes (Figure 5B) highlights the importance of c-Q event analysis at multiple temporal scales. If,
for example, three events each showed a chemostatic response but at different NO₃⁻ concentration, they could be
interpreted as chemodynamic when grouped together. Both methods of analysis could be useful in determining the
275 nutrient export behavior of stormflow events which has been observed to be highly non-linear and hysteretic (Carey
et al., 2014; Lloyd et al., 2016).

3.5 Periods of anomalous flow and NO₃⁻ concentrations can alter overarching riverine c-Q characteristics

During baseflow and stormflow periods, episodes of anomalous flow and NO₃⁻ concentrations had a
280 significant effect on c-Q slope analysis. In *UPN*, two events, during low flow periods in October 2017, had low NO₃⁻
concentrations (average 1.34 and 0.46 mg/L; 4th and 2nd NO₃⁻ concentration percentile across the whole study period,
respectively). Individually, the events had c-Q slopes of -0.50 and 0.45. Inclusion of these events in the calculation of
fall bulk stormflow c-Q behavior resulted in fall bulk stormflow c-Q slope of 0.71 (Figure 4B). However, with the
removal of these events, the same calculation yields a slope of 0.09, much more in line with the other watersheds for
285 the fall season. These events were included in our analysis, as they met the criteria for event selection, however their
ability to skew the bulk analysis is notable as they represent < 1% of annual flow and NO₃⁻ load.

Similarly, during baseflow in *MJF*, a period of anomalously low flow (mean = 96 cfs; < 0.1 flow percentile)
and low nitrate concentration (mean = 0.05 mg/L; < 0.1 NO₃⁻ concentration percentile) from 07/26/2017-10/19/2017



290 had a dramatic impact on the baseflow c-Q relationship (Figure S3D). Inclusion of the data from this period resulted
in an annual baseflow c-Q slope of 1.42, indicating very strong enrichment behavior. Removal of the data from this
anomalous period decreased the slope to 0.42. Data from this time period may be influenced by biofouling, as such
we do not include this period in further discussion of nutrient export behavior, but we do include it in our estimates of
annual and seasonal nitrate load, though it has little effect on our overall load estimates as the amount of nutrient
export during this period is low.

295 The ability of a single anomalous period to influence the overall characterization of a hydrologic system
highlights the difficulty of representing nutrient export behavior based on a single parameter fit across several seasons
and flow regimes (Diamond & Cohen, 2018; Dupas et al., 2017; Marinos et al., 2020). This also highlights the need
for high-frequency data collection activities that allow researchers and water quality practitioners to observe
anomalous events during periods of the year that are not traditionally targeted by discrete or synoptic sampling
300 campaigns.

3.6 Seasonal patterns in nitrate load across watersheds

Annual average NO_3^- export across the study watersheds ranged from 4216 ± 768 kg-N/km²/yr in *USC* to
 2222 ± 371 kg-N/m²/yr in *MRF*. Partitioning the hydrograph into seasonal stormflow and baseflow periods allows the
305 identification of periods which contribute disproportionately to annual watershed NO_3^- export magnitudes (Figure 6).

Spring stormflow periods accounted for the largest contribution to annual load across all watersheds, with an
average of $37.5 \pm 11.5\%$ for all years. Spring stormflow contributions displayed a large spatiotemporal range, from
19.7% in *UPN* in 2016 to 59.8% in *DVM* in 2017. Summer stormflow loads also showed considerable variation, with
an average contribution of 9.4% of annual load, but ranging from < 1% (19.4 kg-N/km²/yr) in 2017 to 18.3% (711 kg-
310 N/km²/yr) in 2018.

These ranges in NO_3^- loads are largely driven by observed variation in summer stormflow events. For
example, in the summer of 2017, which had an anomalously low NO_3^- load, there were fewer stormflow events than
average. Specifically, there was an average of 1.8 events across the watersheds with zero events identified in *USC* and
MJF. In contrast, there was an average of 6.0 events across all five watersheds in summer 2018, which has
315 anomalously high nitrate load. Additionally, the identified events in summer 2017 were approximately 22% the size
of the events in summer 2018. This variability highlights the difficulty in predicting loads across seasons, hydrologic
regimes and watersheds.

Baseflow loads showed considerable variability seasonally, although they consistently made up $\leq 15\%$ of the
annual load in each watershed. Baseflow loads typically peaked in the spring months, likely due to a seasonally high
320 water table, which increased shallow groundwater contribution to streams (Jiang et al., 2010; Molenat et al., 2008).
Additionally, spring fertilizer application and plowing can increase surface leaching, increasing the nitrate pool in the
shallow subsurface (Royer et al., 2006). That said, there were some discrepancies within individual watersheds; *UPN*
had generally higher export in fall baseflow and *MRF* had similar fall and spring loads (Figure 6A).

325



3.7 Nutrient export is driven by the spatial distribution of land use types and hydrologic infrastructure

There is a systematic trend toward higher NO_3^- load in watersheds with a higher density of built drainage infrastructure (Figure 7), consistent with other studies (Basu et al., 2010; Musolff et al., 2015; Schilling & Zhang, 2004). The slope of the relationship between NO_3^- load and drainage infrastructure density is much shallower for baseflow than for stormflow, given the greater range in observed stormflow load across the watersheds (Kennedy et al., 2012). Drainage structures and tile drains route water from high NO_3^- source areas directly to the stream, decreasing travel time and bypassing riparian areas that are highly active in nutrient processing (Dosskey et al., 2010). These structures are common features in agricultural landscapes and show strong correlation to the amount of cropped area across the five watersheds analyzed ($R^2 = 0.95$).

The short circuiting of subsurface flow paths and increased cropped area drives watershed nutrient export patterns towards chemostatic behavior by homogenizing the source regions and limiting nutrient cycling during transport (Marinos et al., 2020; Musolff et al., 2015; Thompson et al., 2011). These patterns are most clear during both baseflow and stormflow periods in the spring months, when tile drains likely have their greatest influence on hydrologic routing. During these periods, stormflow NO_3^- loads are strongly correlated with drainage infrastructure density ($R^2 = 0.88$ and 0.88 , respectively; Table S4) and stormflow export regimes are chemostatic (average c-Q slope = 0.15 for stormflow and 0.18 for baseflow).

In contrast, summer baseflow periods showed the strongest chemodynamic enrichment patterns with an average c-Q slope of 0.73 across all watersheds. The NO_3^- load during these periods is most strongly correlated with the percentage of cropped area within 100 m of the stream ($R^2 = 0.94$; Table S4). This suggests that summer chemodynamic regimes are driven by low flow, low NO_3^- periods where source areas that are proximal to the stream are contributing more significantly to discharge (Molénat et al., 2008). Lower density of agricultural activity in riparian areas (Table S2) leads to more heterogeneous source regions, which promotes low NO_3^- load and the observed chemodynamic behavior.

Seasonal and annual c-Q slopes across all hydrologic regimes show only weak correlations with watershed area suggesting that drainage infrastructure and the distribution and intensity of agriculture are the dominant drivers of NO_3^- export regime in these watersheds. This is consistent with a recent study of 33 agricultural watersheds in the Midwest (Marinos et al., 2020). Our results show that both conditions that lead to high NO_3^- loads, whether hydrologic (i.e. stormflow) or landscape (i.e. increases in drainage infrastructure and agricultural intensity) are associated with chemostatic behavior. This trend is in line with the idea that landscapes with such agricultural intensity are a saturated solute source, whose delivery is flow-limited (Thompson et al., 2011).

4 Conclusions

Detailed analysis of event, seasonal, and annual NO_3^- export showed that all five heavily agricultural watersheds showed similar temporal patterns of NO_3^- load with highs in spring stormflow and lows in summer baseflow. Stormflow across all seasons was largely chemostatic and spring stormflow accounted for ~40% of annual loads. In contrast, baseflow periods exhibited seasonality in export regimes, with low summer flows driving periods of chemodynamic enrichment and winter and spring driving more chemostatic behavior in the winter and spring. The



differences in c-Q behavior between stormflow and baseflow suggests that the systems dynamically, but predictably, shift between NO_3^- export patterns in response to hydrologic forcing. There was a systematic trend toward more chemostatic behavior and higher NO_3^- loads with increasing density of drainage infrastructure and agricultural land use across the five watersheds. These anthropogenic controls on NO_3^- export in these watersheds are driven by disparate glacial histories across the watersheds that necessitate different flow routing infrastructure. During baseflow conditions, land use near the stream has a large impact on NO_3^- loads, indicating that buffer strips or other near-stream management practices may be effective management practices for reducing loads during these periods.

Analysis of specific low-flow periods demonstrated that anomalous periods have the power to significantly affect our classification of export patterns and influence our understanding of watersheds as a whole. This highlights the dynamic nature of these systems and argues for event, seasonal, and longer-term analyses of nutrient export, particularly when attempting to measure the efficacy of management practices such as reductions in fertilizer application or near-stream buffer strips. High-resolution hydrochemical observations allow the detailed characterization of storm events which facilitate more accurate estimates of NO_3^- loads that have been previously measured using regression-based techniques with sparse sample resolution. This study demonstrates the utility of high spatial and temporal resolution water quality sampling to disentangle the key factors controlling watershed nutrient export as well as the important role of state and federal water quality monitoring programs in addressing important water quality issues.

Data availability

Records that have been portioned into stormflow and baseflow for this analysis can be found at <http://www.hydroshare.org/resource/173cff98da3c4263a110cba8c6d62406>.

Author contribution

GG and MZ designed the study, GG carried out the analysis. GG and MZ prepared the manuscript.

Competing interests

The authors declare that they have no conflict of interest.

Acknowledgements

The authors would like to thank the Iowa Institute of Hydraulic Research for generously providing data.

Funding

This work was supported by the National Science Foundation Graduate Research Fellowship Program.

References

Abbott, B. W., Gruau, G., Zarnetske, J. P., Moatar, F., Barbe, L., Thomas, Z., et al. (2018). Unexpected spatial stability of water chemistry in headwater stream networks. *Ecology Letters*, 21(2), 296–308.



- <https://doi.org/10.1111/ele.12897>
- 400 Basu, N. B., Destouni, G., Jawitz, J. W., Thompson, S. E., Loukinova, N. V., Darracq, A., et al. (2010). Nutrient loads exported from managed catchments reveal emergent biogeochemical stationarity. *Geophysical Research Letters*, 37(23), 1–5. <https://doi.org/10.1029/2010GL045168>
- Bieroza, M. Z., Heathwaite, A. L., Bechmann, M., Kyllmar, K., & Jordan, P. (2018). The concentration-discharge slope as a tool for water quality management. *Science of the Total Environment*, 630, 738–749.
- 405 <https://doi.org/10.1016/j.scitotenv.2018.02.256>
- Blaen, P. J., Khamis, K., Lloyd, C., Comer-Warner, S., Ciocca, F., Thomas, R. M., et al. (2017). High-frequency monitoring of catchment nutrient exports reveals highly variable storm event responses and dynamic source zone activation. *Journal of Geophysical Research: Biogeosciences*, 122(9), 2265–2281. <https://doi.org/10.1002/2017JG003904>
- 410 Bouraoui, F., & Grizzetti, B. (2011). Long term change of nutrient concentrations of rivers discharging in European seas. *Science of the Total Environment*, 409(23), 4899–4916. <https://doi.org/10.1016/j.scitotenv.2011.08.015>
- Bowes, M. J., Jarvie, H. P., Halliday, S. J., Skeffington, R. A., Wade, A. J., Loewenthal, M., et al. (2015). Characterising phosphorus and nitrate inputs to a rural river using high-frequency concentration-flow relationships. *Science of the Total Environment*, 511, 608–620. <https://doi.org/10.1016/j.scitotenv.2014.12.086>
- 415 Buda, A. R., & DeWalle, D. R. (2009). Dynamics of stream nitrate sources and flow pathways during stormflows on urban, forest and agricultural watersheds in central Pennsylvania, USA. *Hydrological Processes*, (23), 3292–3305. <https://doi.org/10.1002/hyp.7423>
- Carey, R. O., Wollheim, W. M., Mulukutla, G. K., & Mineau, M. M. (2014). Characterizing storm-event nitrate fluxes in a fifth order suburbanizing watershed using in situ sensors. *Environmental Science and Technology*, 48(14), 7756–7765. <https://doi.org/10.1021/es500252j>
- 420 De Cicco, L. A., Hirsch, R. M., Lorenz, D., & Watkins, W. D. (2018). dataRetrieval: R packages for discovering and retrieving water data available from Federal hydrologic web services. <https://doi.org/10.5066/P9X4L3GE>
- Conley, D. J., Carstensen, J., Aigars, J., Axe, P., Bonsdor, E., Eremina, T., et al. (2011). Hypoxia Is Increasing in the Coastal Zone of the Baltic Sea, 6777–6783. <https://doi.org/10.1021/es201212r>
- 425 Dewitz, J. (2019). *National Land Cover Database (NLCD) 2016 Products: U.S. Geological Survey data release*. <https://doi.org/https://doi.org/10.5066/P96HHBIE>
- Diamond, J. S., & Cohen, M. J. (2018). Complex patterns of catchment solute–discharge relationships for coastal plain rivers. *Hydrological Processes*, 32(3), 388–401. <https://doi.org/10.1002/hyp.11424>
- 430 Diaz, R. J., & Rosenberg, R. (2008). Spreading dead zones and consequences for marine ecosystems. *Science*, 321(5891), 926–929. <https://doi.org/10.1126/science.1156401>
- Dosskey, M. G., Vidon, P., Gurwick, N. P., Allan, C. J., Duval, T. P., & Lowrance, R. (2010). The role of riparian vegetation in protecting and improving chemical water quality in streams. *Journal of the American Water Resources Association*, 46(2), 261–277. <https://doi.org/10.1111/j.1752-1688.2010.00419.x>
- 435 Dupas, R., Jomaa, S., Musolff, A., Borchardt, D., & Rode, M. (2016). Disentangling the influence of hydroclimatic



- patterns and agricultural management on river nitrate dynamics from sub-hourly to decadal time scales. *Science of the Total Environment*, 571(October), 791–800. <https://doi.org/10.1016/j.scitotenv.2016.07.053>
- 440 Dupas, R., Musolff, A., Jawitz, J. W., Rao, P. S. C., Jäger, C. G., Fleckenstein, J. H., et al. (2017). Carbon and nutrient export regimes from headwater catchments to downstream reaches. *Biogeosciences*, 14(18), 4391–4407. <https://doi.org/10.5194/bg-14-4391-2017>
- Dupas, R., Abbott, B. W., Minaudo, C., & Fovet, O. (2019). Distribution of landscape units within catchments influences nutrient export dynamics. *Frontiers in Environmental Science*, 7(APR), 1–8. <https://doi.org/10.3389/fenvs.2019.00043>
- 445 Ehrhardt, S., Kumar, R., Fleckenstein, J. H., Attinger, S., & Musolff, A. (2019). Trajectories of nitrate input and output in three nested catchments along a land use gradient. *Hydrology and Earth System Sciences*, 23(9), 3503–3524. <https://doi.org/10.5194/hess-23-3503-2019>
- Fovet, O., Ruiz, L., Faucheux, M., Molénat, J., Sekhar, M., Vertès, F., & Aquilina, L. (2015). Using long time series of agricultural-derived nitrates for estimating catchment transit times. *Journal of Hydrology*, 522, 603–617. <https://doi.org/10.1016/j.jhydrol.2015.01.030>
- 450 Godsey, S. E. (2009). Concentration-discharge relationships reflect chemostatic characteristics of US catchments. *Hydrological Processes*, (23), 1844–1864. <https://doi.org/10.1002/hyp.7315>
- Hansen, A. T., Dolph, C. L., Fofoula-Georgiou, E., & Finlay, J. C. (2018). Contribution of wetlands to nitrate removal at the watershed scale. *Nature Geoscience*, 11(2), 127–132. <https://doi.org/10.1038/s41561-017-0056-6>
- 455 Hooper, R. P., & Shoemaker, C. A. (1986). A Comparison of Chemical and Isotopic Hydrograph Separation. *Water Resources Research*, 22(10), 1444–1454. <https://doi.org/10.1029/WR022i010p01444>
- Howarth, R. W. (2008). Coastal nitrogen pollution: A review of sources and trends globally and regionally. *Harmful Algae*, 8(1), 14–20. <https://doi.org/10.1016/j.hal.2008.08.015>
- Iowa Nutrient Reduction Strategy: 2018-19 Annual Progress Report*. (2020). Retrieved from <https://store.extension.iastate.edu/product/15915>
- 460 Jenny, J. P., Normandeau, A., Francus, P., Taranu, Z. E., Gregory-Eaves, I., Lapointe, F., et al. (2016). Urban point sources of nutrients were the leading cause for the historical spread of hypoxia across European lakes. *Proceedings of the National Academy of Sciences of the United States of America*, 113(45), 12655–12660. <https://doi.org/10.1073/pnas.1605480113>
- 465 Jiang, R., Woli, K. P., Kuramochi, K., Hayakawa, A., Shimizu, M., & Hatano, R. (2010). Hydrological process controls on nitrogen export during storm events in an agricultural watershed. *Soil Science and Plant Nutrition*, 56(1), 72–85. <https://doi.org/10.1111/j.1747-0765.2010.00456.x>
- Jones, C. S., Wang, B., Schilling, K. E., & Chan, K. sik. (2017). Nitrate transport and supply limitations quantified using high-frequency stream monitoring and turning point analysis. *Journal of Hydrology*, 549(x), 581–591. <https://doi.org/10.1016/j.jhydrol.2017.04.041>
- 470 Kennedy, C. D., Bataille, C., Liu, Z., Ale, S., VanDeVelde, J., Roswell, C. R., et al. (2012). Dynamics of nitrate and chloride during storm events in agricultural catchments with different subsurface drainage intensity (Indiana, USA). *Journal of Hydrology*, 466–467, 1–10. <https://doi.org/10.1016/j.jhydrol.2012.05.002>



- Klaus, J., & McDonnell, J. J. (2013). Hydrograph separation using stable isotopes: Review and evaluation. *Journal of Hydrology*, 505, 47–64. <https://doi.org/10.1016/j.jhydrol.2013.09.006>
- 475 Knapp, J., von Freyberg, J., Studer, B., Kiewiet, L., & Kirchner, J. (2020). Concentration-discharge relationships vary among hydrological events, reflecting differences in event characteristics. *Hydrology and Earth System Sciences Discussions*, 1–27. <https://doi.org/10.5194/hess-2019-684>
- Lloyd, C. E. M., Freer, J. E., Johnes, P. J., & Collins, A. L. (2016). Using hysteresis analysis of high-resolution water quality monitoring data, including uncertainty, to infer controls on nutrient and sediment transfer in catchments. *Science of the Total Environment*, 543, 388–404. <https://doi.org/10.1016/j.scitotenv.2015.11.028>
- 480 Marinos, R. E., Van Meter, K. J., & Basu, N. B. (2020). Is the River a Chemostat?: Scale Versus Land Use Controls on Nitrate Concentration-Discharge Dynamics in the Upper Mississippi River Basin. *Geophysical Research Letters*. <https://doi.org/10.1029/2020gl087051>
- Mellander, P. E., Melland, A. R., Jordan, P., Wall, D. P., Murphy, P. N. C., & Shortle, G. (2012). Quantifying nutrient transfer pathways in agricultural catchments using high temporal resolution data. *Environmental Science and Policy*, 24, 44–57. <https://doi.org/10.1016/j.envsci.2012.06.004>
- 485 Van Meter, K. J., Chowdhury, S., Byrnes, D. K., & Basu, N. B. (2020). Biogeochemical asynchrony: Ecosystem drivers of seasonal concentration regimes across the Great Lakes Basin. *Limnology and Oceanography*, 65(4), 848–862. <https://doi.org/10.1002/lno.11353>
- 490 Minaudo, C., Dupas, R., Gascuel-Oudou, C., Roubeix, V., Danis, P. A., & Moatar, F. (2019). Seasonal and event-based concentration-discharge relationships to identify catchment controls on nutrient export regimes. *Advances in Water Resources*, 131(July), 103379. <https://doi.org/10.1016/j.advwatres.2019.103379>
- Moatar, F., Abbot, B. W., Minaudo, C., Curie, F., & Pinay, G. (2017). Elemental properties, hydrology, and biology interact to shape concentration-discharge curves for carbon, nutrients, sediment, and major ions. *Water Resources Research*, (53), 1270–1287. <https://doi.org/10.1002/2016WR019635>
- 495 Molenat, J., Gascuel-Oudou, C., Ruiz, L., & Gruau, G. (2008). Role of water table dynamics on stream nitrate export and concentration in agricultural headwater catchment (France). *Journal of Hydrology*, 348(3–4), 363–378. <https://doi.org/10.1016/j.jhydrol.2007.10.005>
- Musolff, A., Fleckenstein, J. H., Rao, P. S. C., & Jawitz, J. W. (2017). Emergent archetype patterns of coupled hydrologic and biogeochemical responses in catchments. *Geophysical Research Letters*, 44(9), 4143–4151. <https://doi.org/10.1002/2017GL072630>
- 500 Musolff, Andreas, Schmidt, C., Selle, B., & Fleckenstein, J. H. (2015). Catchment controls on solute export. *Advances in Water Resources*, 86, 133–146. <https://doi.org/10.1016/j.advwatres.2015.09.026>
- Pellerin, B. A., Bergamaschi, B. A., Gilliom, R. J., Crawford, C. G., Saraceno, J., Frederick, C. P., et al. (2014). Mississippi river nitrate loads from high frequency sensor measurements and regression-based load estimation. *Environmental Science and Technology*, 48(21), 12612–12619. <https://doi.org/10.1021/es504029c>
- 505 Peralta-Tapia, A., Sponseller, R. A., Agren, A., Tetzlaff, D., Soulsby, C., & Laudon, H. (2015). Scale-dependent groundwater contributions influence patterns of winter baseflow stream chemistry in boreal catchments. *Journal of Geophysical Research: Biogeosciences*, 120, 847–858.



- 510 <https://doi.org/10.1002/2014JG002878>. Received
- Prior, J. C. (1991). *Landforms of Iowa*. Iowa City, IA: University of Iowa Press.
- Rabalais, N. N., Turner, R. E., & Wiseman, W. J. (2002). Gulf of Mexico hypoxia, a.k.a. “The dead zone.” *Annual Review of Ecology and Systematics*, 33, 235–263. <https://doi.org/10.1146/annurev.ecolsys.33.010802.150513>
- Rabalais, N. N., Turner, R. E., Diaz, R. J., & Justić, D. (2009). Global change and eutrophication of coastal waters. *ICES Journal of Marine Science*, 66(7), 1528–1537. <https://doi.org/10.1093/icesjms/fsp047>
- 515 Richardson, C. M., Zimmer, M. A., Fackrell, J. K., & Paytan, A. (2020). Geologic controls on source water drive baseflow generation and carbon geochemistry: evidence of nonstationary baseflow sources across multiple subwatersheds. *Water Resources Research*.
- Rode, M., Halbedel Née Angelstein, S., Anis, M. R., Borchardt, D., & Weitere, M. (2016). Continuous In-Stream
- 520 Assimilatory Nitrate Uptake from High-Frequency Sensor Measurements. *Environmental Science and Technology*, 50(11), 5685–5694. <https://doi.org/10.1021/acs.est.6b00943>
- Rodríguez-Blanco, M. L., Taboada-Castro, M. M., Taboada-Castro, M. T., & Oropeza-Mota, J. L. (2015). Relating nitrogen export patterns from a mixed land use catchment in NW Spain with rainfall and streamflow. *Hydrological Processes*, 29(12), 2720–2730. <https://doi.org/10.1002/hyp.10388>
- 525 Royer, T. V., David, M. B., & Gentry, L. E. (2006). Timing of riverine export of nitrate and phosphorus from agricultural watersheds in Illinois: Implications for reducing nutrient loading to the Mississippi River. *Environmental Science and Technology*, 40(13), 4126–4131. <https://doi.org/10.1021/es052573n>
- Rozemeijer, J. C., Van Der Velde, Y., Van Geer, F. C., De Rooij, G. H., Torfs, P. J. J. F., & Broers, H. P. (2010). Improving load estimates for NO₃ and P in surface waters by characterizing the concentration response to
- 530 rainfall events. *Environmental Science and Technology*, 44(16), 6305–6312. <https://doi.org/10.1021/es101252e>
- Schilling, K., & Zhang, Y. K. (2004). Baseflow contribution to nitrate-nitrogen export from a large, agricultural watershed, USA. *Journal of Hydrology*, 295(1–4), 305–316. <https://doi.org/10.1016/j.jhydrol.2004.03.010>
- Schilling, K. E., Jindal, P., Basu, N. B., & Helters, M. J. (2012). Impact of artificial subsurface drainage on groundwater travel times and baseflow discharge in an agricultural watershed, Iowa (USA). *Hydrological*
- 535 *Processes*, 26(20), 3092–3100. <https://doi.org/10.1002/hyp.8337>
- Sebilo, M., Mayer, B., Nicolardot, B., Pinay, G., & Mariotti, A. (2013). Long-term fate of nitrate fertilizer in agricultural soils. *Proceedings of the National Academy of Sciences of the United States of America*, 110(45), 18185–18189. <https://doi.org/10.1073/pnas.1305372110>
- Sprague, L. A., Hirsch, R. M., & Aulenbach, B. T. (2011). Nitrate in the Mississippi River and Its Tributaries , 1980
- 540 to 2008 : Are We Making Progress ? *Environmental Science & Technology*, 7209–7216. <https://doi.org/10.1021/es201221s>
- Thompson, S. E., Basu, N. B., Lascrain, J., Aubeneau, A., & Rao, P. S. C. (2011). Relative dominance of hydrologic versus biogeochemical factors on solute export across impact gradients. *Water Resources Research*, 47(7), 1–20. <https://doi.org/10.1029/2010WR009605>
- 545 Turner, R. E., Rabalais, N. N., & Justić, D. (2012). Predicting summer hypoxia in the northern Gulf of Mexico: Redux. *Marine Pollution Bulletin*, 64(2), 319–324. <https://doi.org/10.1016/j.marpolbul.2011.11.008>



Weyer, P. J., Cerhan, J. R., Kross, B. C., Hallberg, G. R., Kantamneni, J., Breuer, G., et al. (2001). Municipal drinking water nitrate level and cancer risk in older women: The Iowa women's health study. *Epidemiology*, 12(3), 327–338. <https://doi.org/10.1097/00001648-200105000-00013>

550 Zimmer, M. A., Pellerin, B., Burns, D. A., & Petrochenkov, G. (2019). Temporal variability in nitrate-discharge relationships in large rivers as revealed by high-frequency data. *Water Resources Research*. <https://doi.org/10.1029/2018WR023478>

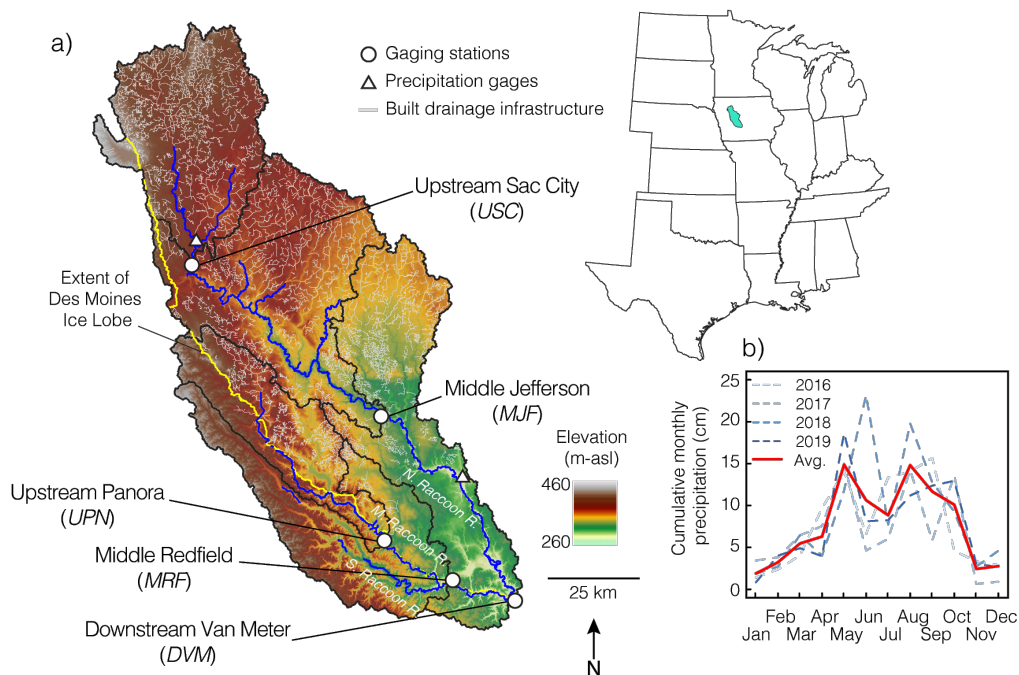
555

560

565

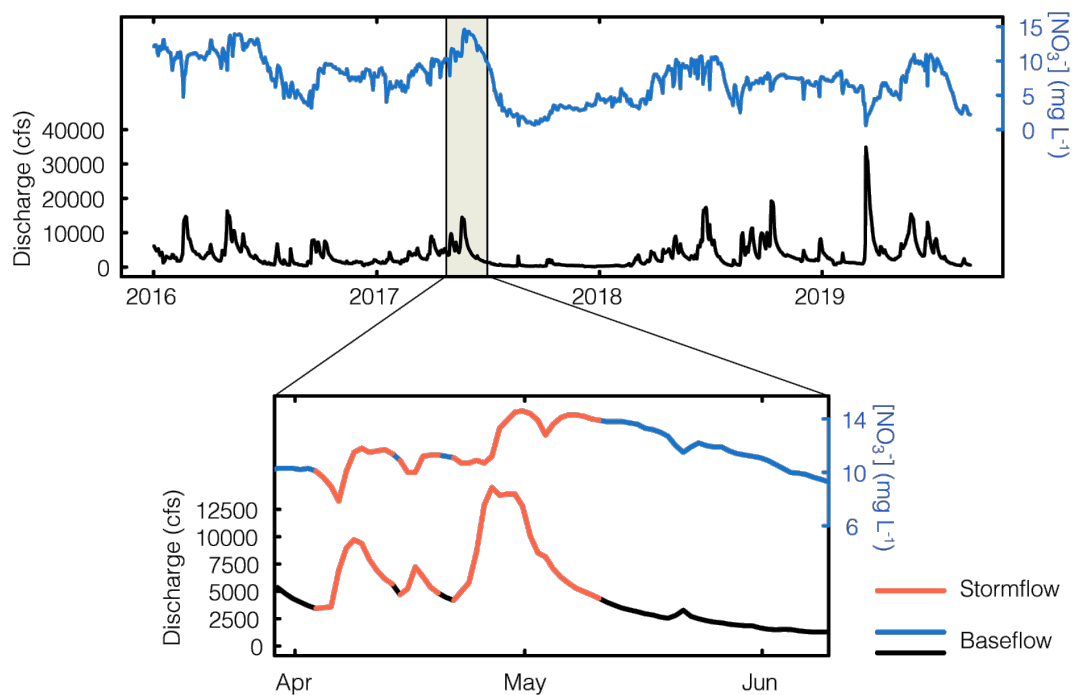
570

575



580 **Figure 1: A) Map of five watersheds (black outlines) analyzed in central Iowa along the North, Middle and South Raccoon Rivers. MJF is inclusive of USC, MRF is inclusive of UPN, and DVM is inclusive of the entire watershed pictured. The yellow line maps the extent of the Des Moines Lobe in the last glaciation. Areas to the southwest of the line lie in the Southern Iowa Drift Plain. Built drainage infrastructure is shown in gray. Gaging stations (white circles) are along the North and Middle Raccoon Rivers (blue lines), the DVM gaging station is below the confluence of the branches of the Raccoon Rivers. Two precipitation gages are shown with white triangles. Precipitation data were averaged on a monthly basis across the four-year study period (2016-2019) and shown in (B); the red line indicates the monthly averages across the four years.**

585



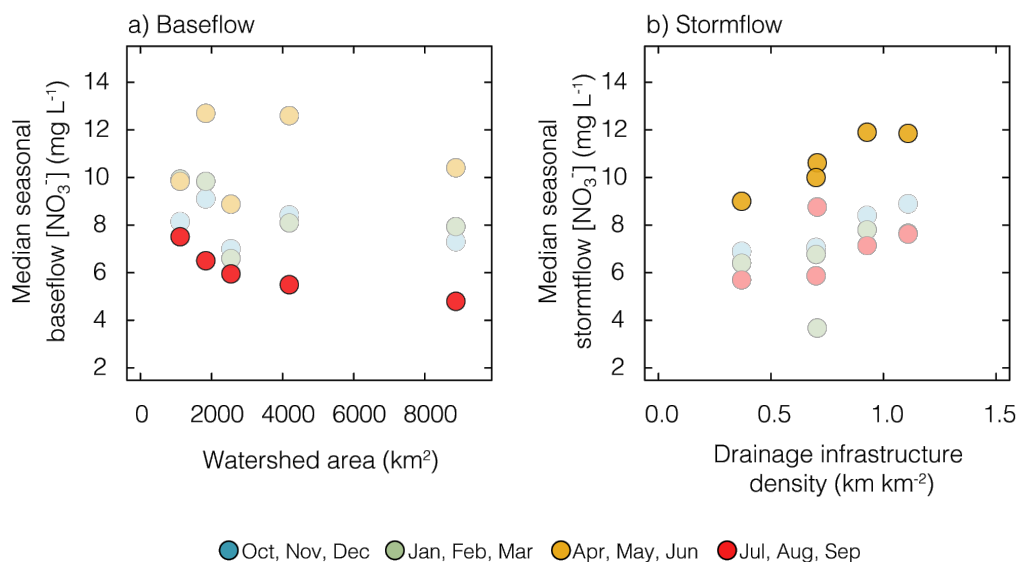
590 **Figure 2:** Example hydrograph and chemograph from one gaging station over the four-year period of analysis, with expanded portion showing stormflow periods (red), and baseflow periods (blue and black). For full records of all five watersheds see Figure S1.



Table 1: Watershed hydrologic characteristics

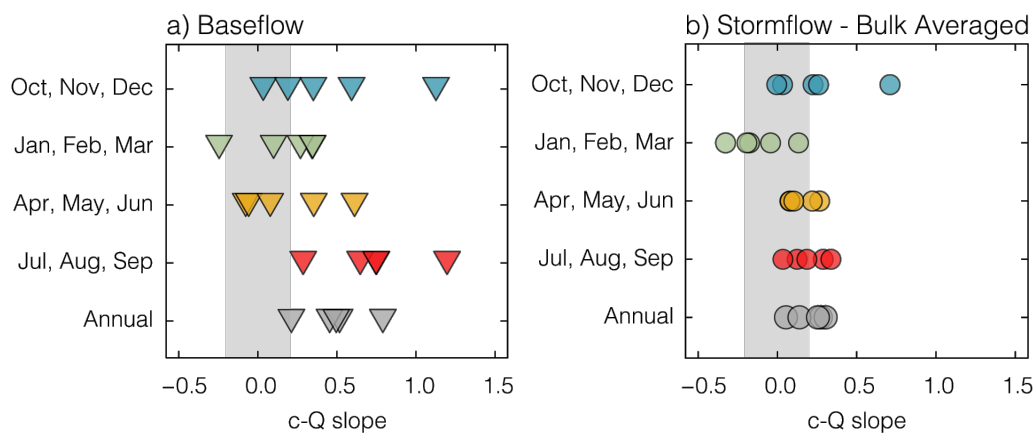
Watershed	Area (km ²)	Stormflow discharge ^a		Stormflow events (events yr ⁻¹)	Stormflow events yr ⁻¹				
		(%)	(%)		Baseflow discharge ^a (%)	OND	JFM	AMJ	JAS
<i>UPN</i>	1116	62.4 (9.3)	32.3 (5.5)	14.3 (1.7)	3.3 (1.5)	1.3 (0.6)	5.0 (0.8)	5.0 (2.2)	5.0 (2.2)
<i>USC</i>	1840	73.4 (3.5)	26.6 (3.6)	15.0 (3.6)	3.0 (1.4)	3.0 (1.8)	5.8 (2.5)	3.3 (2.8)	3.3 (2.8)
<i>MRF</i>	2548	63.3 (4.9)	36.8 (4.1)	16.8 (1.3)	3.8 (1.0)	2.3 (1.0)	5.0 (0.8)	5.8 (1.7)	5.8 (1.7)
<i>MJF</i>	4188	77 (6.1)	23.1 (5.3)	14.3 (3.9)	3.7 (1.6)	2.3 (1.9)	5.5 (1.3)	3.8 (3.3)	3.8 (3.3)
<i>D/M</i>	8870	72.9 (6.7)	27.1 (4.6)	15.8 (5.1)	3.0 (1.9)	2.3 (1.0)	6.3 (1.3)	4.3 (2.8)	4.3 (2.8)

^a as a percent of total annual discharge, standard deviations are reported in parentheses



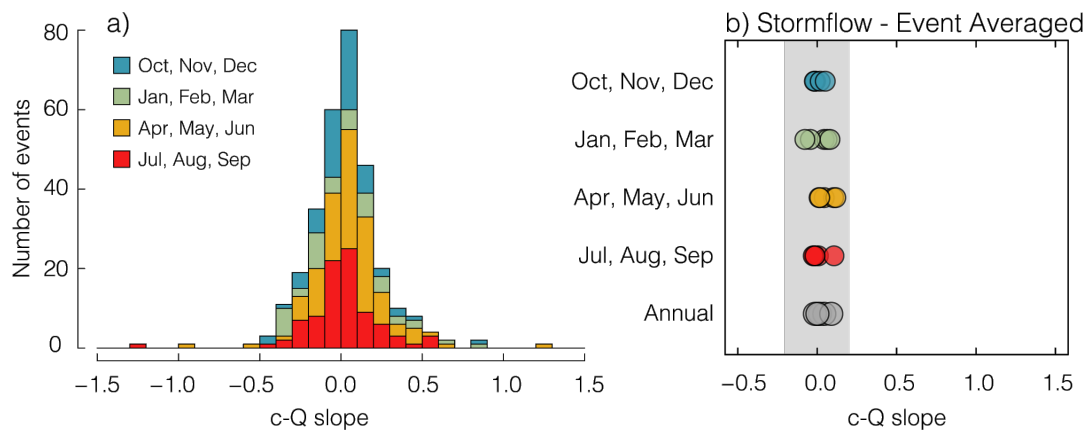
595

Figure 3: Seasonal median NO₃⁻ concentration during baseflow periods plotted against watershed area (A) and NO₃⁻ concentration during stormflow periods plotted against drainage infrastructure density (B). Baseflow NO₃⁻ concentration showed the strongest correlation with watershed area during the summer months (red), and stormflow NO₃⁻ concentration correlated the strongest with drainage infrastructure density during the spring months (yellow).



600

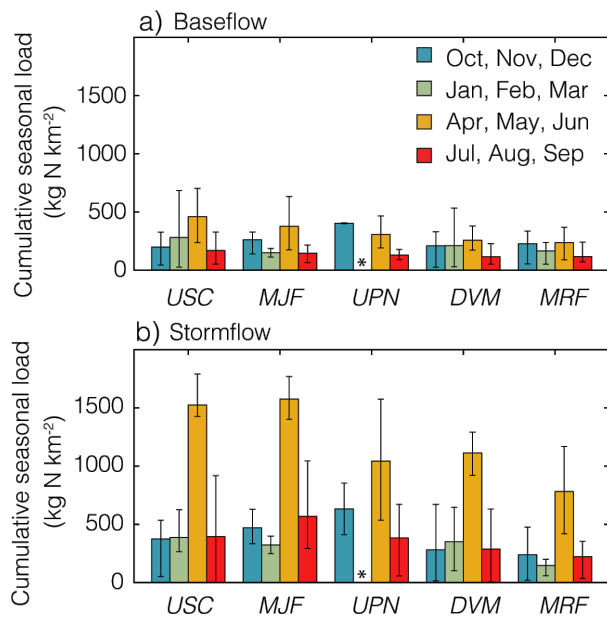
Figure 4: Concentration-discharge slopes in each watershed calculated independently for baseflow (A), and bulk stormflow (B) for each season and annually (gray). Gray boxes indicate chemostatic behavior ($|c-Q \text{ slope}| \leq 0.2$).



605 **Figure 5: (A) Individual storm event c-Q slopes for all five watersheds colored by season, and (B) event averaged stormflow c-Q**
slope by season calculated individually for each watershed, gray boxes indicate chemostatic behavior ($|c-Q \text{ slope}| \leq 0.2$).

610

615



620 **Figure 6: Seasonal NO_3^- load (kg-N/km²) normalized by watershed area, averaged over the four years of analysis (2016-2019) for each watershed for baseflow periods (A) and stormflow periods (B). Watersheds are ordered by the density of drainage infrastructure from highest (USC) to lowest (MRF). Error bars show the range of loads measured over the four-year period. Insufficient data were available to estimate winter loads in UPN indicated with (*).**

625

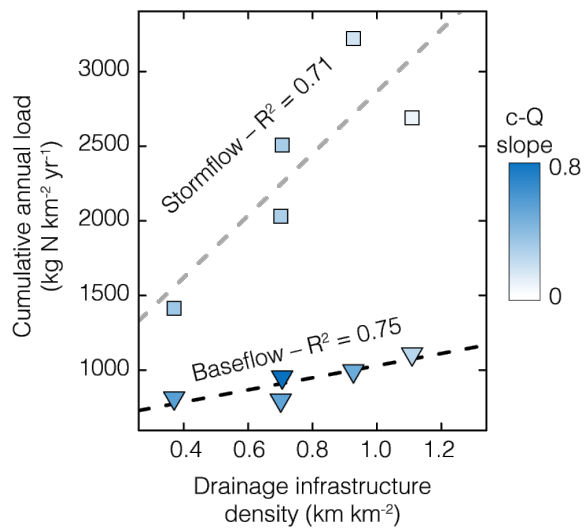


Figure 7: For all five watersheds, cumulative annual load exported during stormflow (squares) and baseflow (triangles) periods as a function of the drainage infrastructure density. Shapes are colored by the average c-Q slope for stormflow and baseflow periods with darker blues associated with more chemodynamic export regimes.

630